Numerical Calculation of the Dielectric and Electrokinetic Properties of Vesicle Suspensions

Constantino Grosse*,†,‡ and Viviana Zimmerman†

Departamento de Física, Universidad Nacional de Tucumán, Av. Independencia 1800, (4000) S.M. de Tucumán, Argentina, and Consejo Nacional de Investigaciones Científicas y Técnicas, Argentina

Received: June 8, 2005; In Final Form: August 3, 2005

The dielectric and electrokinetic properties of aqueous suspensions of vesicles (unilamellar liposomes) are numerically calculated in the 1 Hz to 1 GHz frequency range using a network simulation method. The model consists of a conducting internal medium surrounded by an insulating membrane with fixed surface charges on both sides. Without an applied field, the internal medium is in electric equilibrium with the external one, so that it also bears a net volume charge. Therefore, in the presence of an applied ac field, there is fluid flow both in the internal and in the external media. The obtained results are qualitatively different from those corresponding to suspensions of charged homogeneous particles, mainly due to the existence of an additional length scale (the membrane thickness) and the corresponding dispersion mechanism, charging of the membrane. Because of this dispersion, the shapes of the spectra change with the size of the particles (at constant ζ potential and particle radius to Debye length ratio) instead of merely shifting along the frequency axis. A comparison between the numerical results and those obtained using approximate analytical expressions shows deviations that are, in general, sufficiently large enough to show the necessity to use numerical results in order to interpret broad frequency range dielectric and electrokinetic measurements of vesicle suspensions.

Introduction

Most of the numerical studies on dielectric and electrokinetic properties of colloidal suspensions deal with homogeneous insulating particles, such as latex, alumina, or silica.[1−4] In more recent works, particles coated with a permeable membrane (soft particles) have also been extensively investigated.[5−13] However, there are practically no numerical studies of suspensions of inhomogeneous particles, such as a conducting core surrounded by an insulating membrane, despite the obvious importance of such systems that can be used as a basis for the modeling of biological systems.

In two recent works[14,15] we presented numerical studies of the dielectric and electrokinetic properties of cell suspensions, using a model consisting of a conducting internal medium surrounded by an insulating membrane and an ion permeable wall. In that model, which could be appropriate for some biological cells, it was assumed that the electric charge of the cell was made of a free volume charge density located in the inner medium and a fixed charge density uniformly distributed over the cell wall. It was considered, moreover, that due to a possible structure in the internal part of the cell, there was no fluid flow in the inner medium.

In the present work we apply the same numerical method for the study of vesicle suspensions. The model used for these systems is simpler than that for cells since there is no cell wall. However, the internal medium in a vesicle is made of the same electrolyte solution as the surrounding medium, so that it is free to move in response to an applied field. This internal fluid flow is qualitatively similar to the flow inside a closed electrophoretic cell.

* To whom correspondence should be addressed. E-mail: cgrosse@herrera.unt.edu.ar.

† Universidad Nacional de Tucumán.

‡ Consejo Nacional de Investigaciones Científicas y Técnicas.

Numerical Calculations

The suspended vesicle is modeled as a spherical volume of electrolyte solution with radius $a - h$, surrounded by an insulating shell with thickness h representing the membrane. The membrane bears uniform surface charge distributions on both sides. In view of this fixed surface charge, the internal medium acquires a volume distribution of free charge of opposite sign.[14−16] This charge can be thought of as due to counterions trapped inside the membrane when the vesicle is formed or as the result of an electric current slowly leaking through the membrane until the equilibrium state is reached.

We further assume, as usual, that there are only two types of ions in the solution, that the permittivity and viscosity have constant values throughout the solution up to the inner or outer surfaces of the membrane, and that there are no dissociation or recombination phenomena. For the sake of simplicity, and in order to be able to compare the obtained results with analytical expressions, we further assume that the ions are univalent.

According to these hypotheses, the electric potential $\phi(\vec{r},t)$, the ion number concentrations of positive and negative ions $C^{\pm}(\vec{r},t)$, and the fluid velocity $\vec{v}(\vec{r},t)$ are obtained solving the following equation system:

Laplace equation ($a - h < r < a$)

$$\nabla^2\phi = 0$$

Poisson equation ($0 < r < a - h$, $a < r < \infty$)

$$\nabla^2\phi = \frac{e}{\epsilon_e}(C^+ - C^-)$$

10.1021/jp053074b CCC: $30.25
Published on Web 09/03/2005

Nernst−Planck equation ($0 < r < a - h$, $a < r < \infty$)

$$\vec{J}^{\pm} = -D^{\pm}\nabla C^{\pm} \mp \frac{eD^{\pm}}{kT} C^{\pm}\nabla\phi + C^{\pm}\vec{v}$$

Continuity equation ($0 < r < a - h$, $a < r < \infty$)

$$\nabla.\vec{J}^{\pm} = -\frac{\partial C^{\pm}}{\partial t}$$

Navier−Stokes equation ($0 < r < a - h$, $a < r < \infty$)

$$\eta\nabla^2\vec{v} - \nabla p = e(C^{+} - C^{-})\nabla\phi + \rho_e\left[\frac{\partial\vec{v}}{\partial t} + (\vec{v}\cdot\nabla)\vec{v}\right]$$

Incompressibility equation ($0 < r < a - h$, $a < r < \infty$)

$$\nabla\cdot\vec{v} = 0$$

where $p(\vec{r},t)$ is the pressure, $D^{\pm}$ and $\vec{J}^{\pm}(\vec{r},t)$ the diffusion coefficients and fluxes of positive and negative ions, η, ρ_e, and ϵ_e the viscosity, mass density, and absolute permittivity of the electrolyte solution, e the elementary charge, k Boltzmann's constant, and T the temperature. In the equation system, the explicit dependence with the variables $(\vec{r},t)$ is omitted in order to simplify the notation.

To solve this equation system, it is first separated into equilibrium and nonequilibrium parts. The nonequilibrium part is further simplified by keeping only linear terms in the applied field. The resulting equation systems and boundary conditions used in their solution are given in ref 14. Here we shall only show the new boundary conditions used in the inner medium, in view of the existence of a field-induced fluid flow that was not considered in previous calculations.

Radial Component of the Velocity. The nonslipping condition on the inner surface of the impermeable membrane together with symmetry considerations lead to

$$\frac{\partial v_r(r,t)}{\partial r}|_{r=0} = 0$$

$$v_r(a - h,t) = 0$$

Vorticity. The vorticity, defined as $\vec{b}(r,t) = \text{curl } \vec{v}(r,t)$, vanishes at the center of the vesicle in view of symmetry considerations. On the other hand, its value at the inner membrane interface is obtained starting with the balance of forces acting on the membrane

$$\vec{F}_{mech}|_{a+} + \vec{F}_{mech}|_{(a-h)-} + \vec{F}_{elec}|_{a+} + \vec{F}_{elec}|_{(a-h)-} = \frac{4\pi}{3}[a^3 - (a - h)^3]\rho_m\frac{\partial\vec{v}(a,t)}{\partial t}$$

where ρ_m is the mass density of the membrane. The first two addends in this expression represent the total mechanical force (due to pressure and viscous contributions) so that they are calculated by integrating the stress tensor over the outer and inner surfaces of the membrane. The next two addends represent the electrical force, which is calculated as minus the electrical force acting on the volume charge densities both in the inner medium and outside the particle, in view of the electroneutrality of the whole system. Combining this expression with the balance of forces written for the whole particle

$$\vec{F}_{mech}|_{a+} + \vec{F}_{elec}|_{a+} = \frac{4\pi}{3}\{(a - h)^3\rho_e + [a^3 - (a - h)^3]\rho_m\}\frac{\partial\vec{v}(a,t)}{\partial t} \quad (1)$$

leads to

$$\vec{F}_{mech}|_{(a-h)-} + \vec{F}_{elec}|_{(a-h)-} = -\frac{4\pi}{3}(a - h)^3\rho_e\frac{\partial\vec{v}(a,t)}{\partial t} \quad (2)$$

and to the final expression for the boundary condition

$$b(a - h,t) - (a - h)\frac{\partial b(r,t)}{\partial r}|_{a-h} = -\frac{kT}{(a - h)^2\eta}\int_0^{a-h}(C_0^{+}\delta\tilde{\mu}^{+} - C_0^{-}\delta\tilde{\mu}^{-})\frac{d\tilde{\phi}_0}{dr}r^2\,dr$$

Here $\delta\tilde{\mu}^{\pm}(r,t)$ are the dimensionless electrochemical potentials[17−19]

$$\delta\tilde{\mu}^{\pm} = \frac{\delta C^{\pm}}{C_0^{\pm}} \pm \delta\tilde{\phi}$$

the lower index 0 represents the equilibrium situation (no applied field), and the δ symbol stands for the variations with respect to equilibrium.

This boundary condition is analogous to the condition for the vorticity in the outer medium,[14] which is deduced starting with eq 1 instead of eq 2

$$b(a,t) - a\frac{\partial b(r,t)}{\partial r}|_{a+} = a\frac{\Delta\rho}{\eta}\frac{\partial v_r(a,t)}{\partial t} + \frac{kT}{a^2\eta}\int_a^{\infty}(C_0^{+}\delta\tilde{\mu}^{+} - C_0^{-}\delta\tilde{\mu}^{-})\frac{d\tilde{\phi}_0}{dr}r^2\,dr$$

where

$$\Delta\rho = \frac{a^3 - (a - h)^3}{a^3}(\rho_m - \rho_e)$$

is the difference between the average mass density of the whole particle and the mass density of the electrolyte solution.

Analytical Expressions

To help the interpretation of the numerical results, analytical expressions for the different properties were deduced.

High-Frequency Dipolar Coefficient. While no rigorous analytical expression for the high-frequency response of a suspended charged particle exists, an approximate expression can be obtained by solving the Laplace equation. The model is the same as the one used in the numerical calculations, except for the equilibrium volume charge densities that are represented by surface conductivities λ on both sides of the membrane.

The complex equivalent conductivity of the vesicle can be determined using the Maxwell mixture formula

$$K_v^{*} = L_e + K_m^{*}\frac{K_i^{*} + 2K_m^{*} + 2p(K_i^{*} - K_m^{*})}{K_i^{*} + 2K_m^{*} - p(K_i^{*} - K_m^{*})} = L_e + i\omega\left(\frac{G_v}{1 + i\omega\tau_v} + \epsilon_{v\infty}\right) \quad (3)$$

where

$$L_e = \frac{2\lambda}{a} \quad K_m^* = i\omega\epsilon_m \quad K_i^* = \sigma_i + L_i + i\omega\epsilon_i$$

$$L_i = \frac{2\lambda}{a-h} \quad p = \frac{(a-h)^3}{a^3}$$

The symbol σ denotes the conductivites, and the lower indexes m, i, and e stand for membrane, internal, and external media. The resulting relaxation parameters of the vesicle are

$$G_v = \frac{9p\epsilon_m{}^2}{(1-p)[\epsilon_i + 2\epsilon_m - p(\epsilon_i - \epsilon_m)]}$$

$$\tau_v = \frac{3\epsilon_m + (\epsilon_i - \epsilon_m)(1-p)}{(\sigma_i + L_i)(1-p)}$$

$$\epsilon_{v\infty} = \epsilon_m \frac{\epsilon_i + 2\epsilon_m + 2p(\epsilon_i - \epsilon_m)}{\epsilon_i + 2\epsilon_m - p(\epsilon_i - \epsilon_m)}$$

The high-frequency dipolar coefficient of the suspended vesicle is determined as

$$d_H^* = \frac{K_v^* - K_e^*}{K_v^* + 2K_e^*} = \frac{G_\beta}{1 + i\omega\tau_\beta} + \frac{G_\delta}{1 + i\omega\tau_\delta} + d_{H\infty} \qquad (4)$$

where

$$K_e^* = \sigma_e + i\omega\epsilon_e$$

The resulting high-frequency dispersion parameter values of the suspension are

$$G_\beta = \frac{G_v\tau_\beta + (\tau_v - \tau_\beta)[\tau_\beta(L_e - \sigma_e) - \epsilon_{v\infty} + \epsilon_e]}{\tau_\beta(L_e + 2\sigma_e)(\tau_\delta - \tau_\beta)}$$

$$\tau_\beta = \frac{\tau_v + \tau_l + \tau_h + \sqrt{(\tau_v + \tau_l + \tau_h)^2 - 4\tau_v\tau_h}}{2}$$

$$G_\delta = \frac{G_v\tau_\delta + (\tau_v - \tau_\delta)[\tau_\delta(L_e - \sigma_e) - \epsilon_{v\infty} + \epsilon_e]}{\tau_\delta(L_e + 2\sigma_e)(\tau_\beta - \tau_\delta)}$$

$$\tau_\delta = \frac{\tau_v + \tau_l + \tau_h - \sqrt{(\tau_v + \tau_l + \tau_h)^2 - 4\tau_v\tau_h}}{2}$$

where

$$\tau_l = \frac{G_v}{L_e + 2\sigma_e} \qquad \tau_h = \frac{\epsilon_{v\infty} + 2\epsilon_e}{L_e + 2\sigma_e}$$

$$d_{H\infty} = \frac{\epsilon_{v\infty} - \epsilon_e}{\epsilon_{v\infty} + 2\epsilon_e} \qquad \epsilon_{v\infty} = \epsilon_m \frac{\epsilon_i + 2\epsilon_m + 2p(\epsilon_i - \epsilon_m)}{\epsilon_i + 2\epsilon_m - p(\epsilon_i - \epsilon_m)}$$

and the lower indexes β and δ stand for the corresponding relaxations.

Low-Frequency Dipolar Coefficient. The expression for the low-frequency dipolar coefficient of a homogeneous, charged, insulating particle, suspended in an univalent electrolyte solution, is, according to the Shilov−Dukhin theory[17,18]

$$d_L^* = G_\alpha \frac{1 + \sqrt{\frac{2}{S}}\sqrt{i\omega\tau_\alpha}}{1 + \sqrt{\frac{2}{S}}\sqrt{i\omega\tau_\alpha} + i\omega\tau_\alpha} + d_{L\infty} \qquad (5)$$

where

$$G_\alpha = -\frac{\frac{3}{2}\frac{(R^+ - R^-)^2}{R+2}\frac{4D^+D^-}{(D^+ + D^-)^2}}{(R^+ + 2)(R^- + 2 - U^-) + (R^- + 2)(R^+ + 2 - U^+)}$$

$$S = \frac{R+2}{(R^+ + 2)(R^- + 2 - U^-) + (R^- + 2)(R^+ + 2 - U^+)}$$

$$\tau_\alpha = \frac{Sa^2(D^+ + D^-)}{4D^+D^-} \qquad (6)$$

$$d_{L\infty} = \frac{R-1}{R+2}$$

$$R = \frac{R^+D^+}{D^+ + D^-} + \frac{R^-D^-}{D^+ + D^-}$$

$$R^\pm = \frac{2G_0^\pm}{aC(\infty)} + 6m^\pm\left[\frac{G_0^\pm}{aC(\infty)} \pm \frac{\tilde{\zeta}}{\kappa a}\right]$$

$$U^\pm = \frac{48m^\pm}{\kappa a}\ln\left(\cosh\frac{\tilde{\zeta}}{4}\right)$$

$$m^\pm = \frac{2\epsilon_e}{3\eta D^\pm}\left(\frac{kT}{e}\right)^2 \qquad (7)$$

$$\kappa = \sqrt{\frac{2e^2C(\infty)}{kT\epsilon_e}} \qquad (8)$$

$$G_0^\pm = \frac{2C(\infty)}{\kappa}(e^{\mp\tilde{\zeta}/2} - 1) \qquad (9)$$

and $C(\infty)$ is the counterion or co-ion concentration far from any particle.

General Expression for the Dipolar Coefficient. A general expression for the dipolar coefficient, valid in the whole frequency range, can be obtained by replacing $d_{L\infty}$ in eq 5 with eq 4

$$d^* = G_\alpha \frac{1 + \sqrt{\frac{2}{S}}\sqrt{i\omega\tau_\alpha}}{1 + \sqrt{\frac{2}{S}}\sqrt{i\omega\tau_\alpha} + i\omega\tau_\alpha} + \frac{G_\beta}{1 + i\omega\tau_\beta} + \frac{G_\delta}{1 + i\omega\tau_\delta} + d_{H\infty} \qquad (10)$$

This substitution requires that the high-frequency limit of eq 5 coincides with the low-frequency limit of eq 4,[20]

$$d_{L\infty} = \frac{R-1}{R+2} = d_H(0) = \frac{L_e - \sigma_e}{L_e + 2\sigma_e}$$

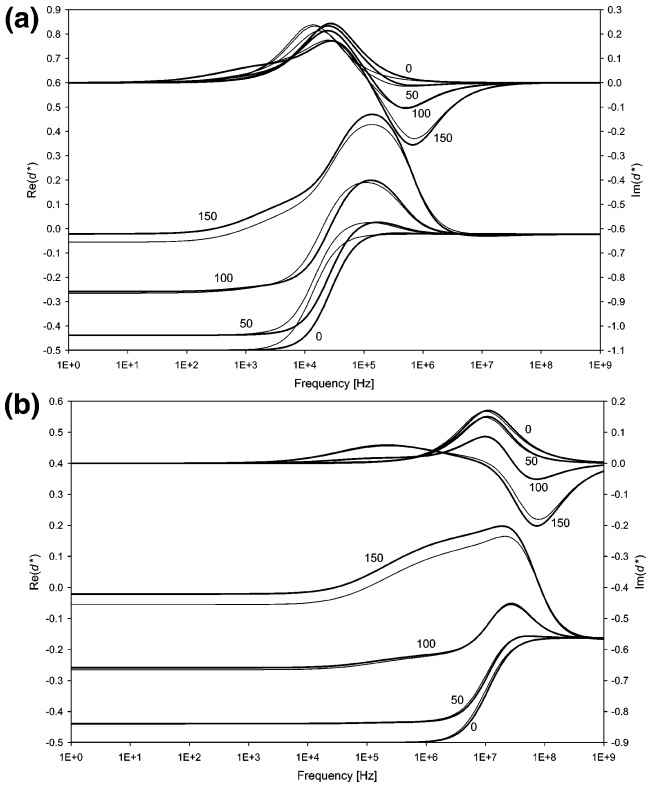

Figure 1. (a) Real (lower curves) and imaginary (upper curves) parts of the dipolar coefficient of large vesicles ($a = 1\ \mu$m) calculated for the indicated values of the ζ potential (in mV) and for $\kappa a = 32$. Numerical results (heavy lines) and analytical results (thin lines), eq 10, are shown. Remaining parameters are given in Table 1. (b) Same as part a but for small vesicles ($a = 100$ nm).

which determines the value of the surface conductivity

$$\frac{2\lambda}{a\sigma_e} = R$$

Furthermore, the electrolyte solution conductivity used in the high-frequency model must be expressed in terms of the parameters defining the low-frequency one

$$\sigma_e = \sigma_i = \frac{C(\infty)e^2(D^+ + D^-)}{kT} \qquad (11)$$

Results and Discussion

Numerical calculations were made using ζ and κa as free parameters considering, furthermore, two different values for the vesicle radius: $a = 1\ \mu$m and $a = 100$ nm. It is well-known that, at constant κa, this last parameter has no bearing on the dielectric spectra of suspensions made of charged homogeneous particles: For larger particles the spectra merely shift to lower frequencies.[21] However, this is not the case for inhomogeneous particles due to the additional dispersion term related to the charging of the membrane, β relaxation. This happens because the corresponding relaxation time τ_β is roughly proportional to the radius of the particle[22] instead of its square as is the case for the low-frequency dielectric dispersion; see eq 6. The parameters used in the calculations are given in Table 1.

Dipolar Coefficient. The obtained results for the real and imaginary parts of the dipolar coefficient calculated as a function of the ζ potential and for $\kappa a = 32$ are represented in Figure 1. Figure 1a, which corresponds to $a = 1\ \mu$m, shows that, for an uncharged particle, the system undergoes just one relaxation,

TABLE 1: Parameter Values Used in All the Calculations

$T = 298.4$ K	$\eta = 8.904 \times 10^{-4}$ Poise
$\epsilon_i = \epsilon_e = 78.36\ \epsilon_0$	$\epsilon_m = 6.0\ \epsilon_0$
$h = 50 \times 10^{-10}$ m	$D^+ = D^- = 2.0 \times 10^{-9}$ m^2 s^{-1}
$\rho_e = 1000$ kg m^{-3}	$\rho_m = 850$ kg m^{-3}

the β process, associated with the charging of the membrane. Actually there is also a δ process, associated with the Maxwell−Wagner polarization of the whole particle, but its amplitude is negligible because the dielectric properties of the uncharged vesicle are almost identical to those of the surrounding medium. When the charge of the particle is increased, the amplitude of this high-frequency relaxation also increases due to the increasing effective conductivity of the particle, eq 3, while the amplitude of the β relaxation decreases due to the electrical shielding of the membrane. At the same time, the low-frequency α dispersion also increases as can be clearly seen for the $\zeta = 150$ mV curves. It is to be noted that, despite the relatively high value, $\kappa a = 32$, there is a large discrepancy between the analytical and numerical results in the frequency range of the β dispersion. This happens because the Debye screening length, despite being much smaller than the particle radius, is actually larger than the membrane thickness. Therefore, the effective thickness of the membrane is larger than the theoretical one,[23,24] so that the membrane capacity and the associated relaxation time are lower. Furthermore, for $\zeta = 150$ mV, the low-frequency limit of the dipolar coefficient does not coincide with the analytical prediction. This is a well-known limitation of the theoretical model[25] with no clear explanation to date.

These same considerations generally apply to Figure 1b, which corresponds to $a = 100$ nm. As expected, the low- and the high-frequency relaxations are merely shifted two decades higher in frequency. However, the medium-frequency β relaxation shifts up nearly three decades, because the corresponding relaxation time is roughly proportional to the radius of the particle divided by the electrolyte solution conductivity[22] and σ_e is proportional to κ^2, eqs 8 and 11, so that τ_β increases with the cube of the radius at constant κa. Another difference with respect to Figure 1a is the good agreement between the analytical and numerical curves in the frequency range of the β relaxation. This is a consequence of decreasing the radius at constant κa, which leads to a Debye screening length that is smaller than the thickness of the membrane.

Figure 2a, which corresponds to $a = 1\ \mu$m, shows the dependence of the dipolar coefficient on the product κa, while the ζ potential is kept at a constant value of 50 mV. Under these conditions, when the value of κa decreases, the agreement between analytical and numerical results worsens due to two main factors. The first is the increment of the effective membrane thickness and the corresponding decrement of the membrane capacity. This change shifts the β relaxation to higher frequencies separating more and more the numerical and analytical curves in the frequency range of the β dispersion. Furthermore, it diminishes the corresponding relaxation amplitude. The second is the strong increment, with respect to the analytical value, of the real part of the dipolar coefficient at low frequencies, which occurs when the Debye length becomes comparable to the radius of the particle and is caused by the growth of the effective particle radius.[21,26]

The same arguments generally apply to Figure 2b, which corresponds to $a = 100$ nm. However, the agreement between analytical and numerical results is much better because the Debye lengths are smaller, so that the membrane capacities are better represented by the theoretical values. Anyway, this partial agreement breaks down for the lowest values of κa, as expected.

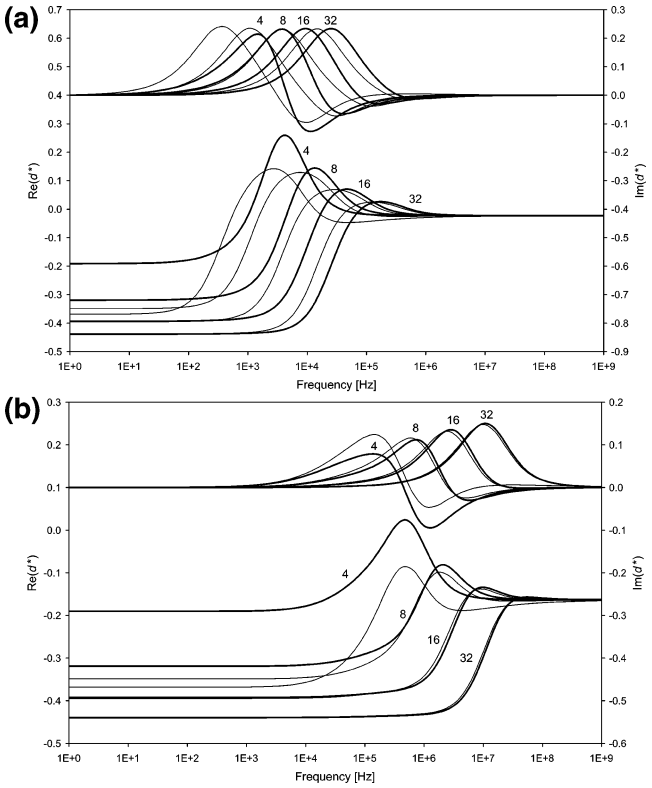

Figure 2. (a) Real (lower curves) and imaginary (upper curves) parts of the dipolar coefficient of large vesicles ($a = 1\ \mu$m) calculated for the indicated values of the product κa and for $\zeta = 50$ mV. Numerical results (heavy lines) and analytical results (thin lines), eq 10, are shown. Remaining parameters are given in Table 1. (b) Same as part a but for small vesicles ($a = 100$ nm).

Permittivity and Conductivity Increments. Numerical permittivity and conductivity values were calculated using the general expressions, valid for small values of the volume fraction v of particles in the suspension

$$\epsilon = \epsilon_e + 3v\epsilon_e\left(d' + \frac{\sigma_e}{\omega\epsilon_e}d''\right) \tag{12}$$

$$\sigma = \sigma_e + 3v\sigma_e\left(d' - \frac{\omega\epsilon_e}{\sigma_e}d''\right) \tag{13}$$

When these equations are used together with the analytical expression for the dipolar coefficient, one difficulty arises: the limiting high-frequency form of the imaginary part of the low-frequency expression of the dipolar coefficient is proportional to $\omega^{-1/2}$; see eq 5. This behavior, which is due to the use of the hypothesis of local equilibrium in the double layer that ceases to be valid at high frequencies,[20] leads to a conductivity expression that becomes proportional to $\omega^{1/2}$ for $\omega \to \infty$, instead of a constant value independent of ω.

To deal with this problem, the usual approximation was used:[21,27] It was considered that only the imaginary part of the low-frequency dipolar coefficient enters in the permittivity expression (eq 12), and correspondingly, only the real part of the low-frequency dipolar coefficient enters in the conductivity expression (eq 13)

$$\epsilon = \epsilon_e + 3v\epsilon_e\left[d_H' + \frac{\sigma_e}{\omega\epsilon_e}(d_L'' + d_H'')\right]$$

$$\sigma = \sigma_e + 3v\sigma_e\left[d_L' - d_{L\infty} + d_H' - \frac{\omega\epsilon_e}{\sigma_e}d_H''\right] \tag{14}$$

It is worth noting that these equations can be combined leading to the following expression for the complex conductivity of the suspension

$$\frac{K^* - K_e^*}{3v} = \frac{\sigma(0) - \sigma_e}{3v} + i\omega\epsilon_e\left\{\frac{-G_\alpha\frac{\tau_\alpha}{\tau_e}}{1 + \sqrt{\frac{2}{S}}\sqrt{i\omega\tau_\alpha} + i\omega\tau_\alpha} + \frac{G_\beta\left(1 - \frac{\tau_\beta}{\tau_e}\right)}{1 + i\omega\tau_\beta} + \frac{G_\delta\left(1 - \frac{\tau_\delta}{\tau_e}\right)}{1 + i\omega\tau_\delta} + d_{H\infty}\right\} \tag{15}$$

where

$$\frac{\sigma(0) - \sigma_e}{3v} = \sigma_e d_L(0)$$

$$\tau_e = \frac{\epsilon_e}{\sigma_e}$$

$$K^* = \sigma + i\omega\epsilon$$

Except for the presence of the two high-frequency dispersion terms, eq 15 has exactly the same form as the empirical expression proposed by Nettelblad and Niklasson[28] for the description of the low-frequency dielectric dispersion of colloidal suspensions.

Figure 3 shows the obtained results for the relative permittivity and conductivity increments calculated as a function of the ζ potential and for $\kappa a = 32$. The most striking feature of Figure 3a, which corresponds to $a = 1\ \mu$m particles, is the sharp drop at high frequencies of the conductivity for suspensions of particles with the highest charge. While this phenomenon has already been numerically calculated for polymer-coated and bare-latex particle suspensions,[12,29] it is particularly strong in the considered case. While a full understanding of this phenomenon would require a specific study in which all the intervening parameters are varied, it is certainly related to inertial effects and their influence on the dipolar coefficient. Due to fluid inertia, the contribution of the electro-osmotic tangential fluid flow to the field-induced dipole moment should diminish in amplitude and change phase (the capillary-osmotic flow is negligible at these frequencies). Furthermore, the contribution of the electrophoretic motion of the particle to the field-induced dipole moment should also diminish in amplitude and change phase.

As for the other features of the curves, Figure 3a shows that the agreement between the analytical and numerical results is generally quite poor. For highly charged particles, it is poor at low frequencies because of the above-mentioned limitations of the theoretical model. For weakly charged particles, the agreement at low frequencies becomes even worse for the permittivity, because of the overestimated contribution of the β relaxation in the analytical results and the fact that the low-frequency limit of the permittivity, unlike the dipolar coefficient, depends on all the dispersion processes, since it is related to the field-induced energy stored in the system.[30,31] On the contrary, the low-frequency agreement of the conductivity greatly improves because for these frequencies the conductivity only depends on the real part of the dipolar coefficient, eq 13

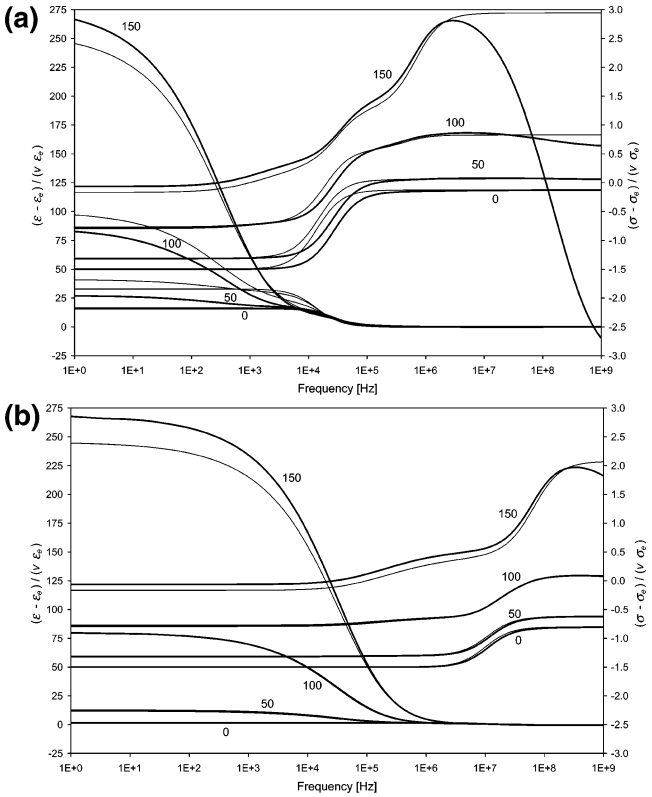

Figure 3. (a) Relative permittivity (decreasing curves) and conductivity (increasing curves) increments of suspensions of large vesicles (a = 1 μm) calculated for the indicated values of the ζ potential (in mV) and for $\kappa a = 32$. Numerical results (heavy lines) and analytical results (thin lines), eq 14, are shown. Remaining parameters are given in Table 1. (b) Same as part a but for small vesicles (a = 100 nm).

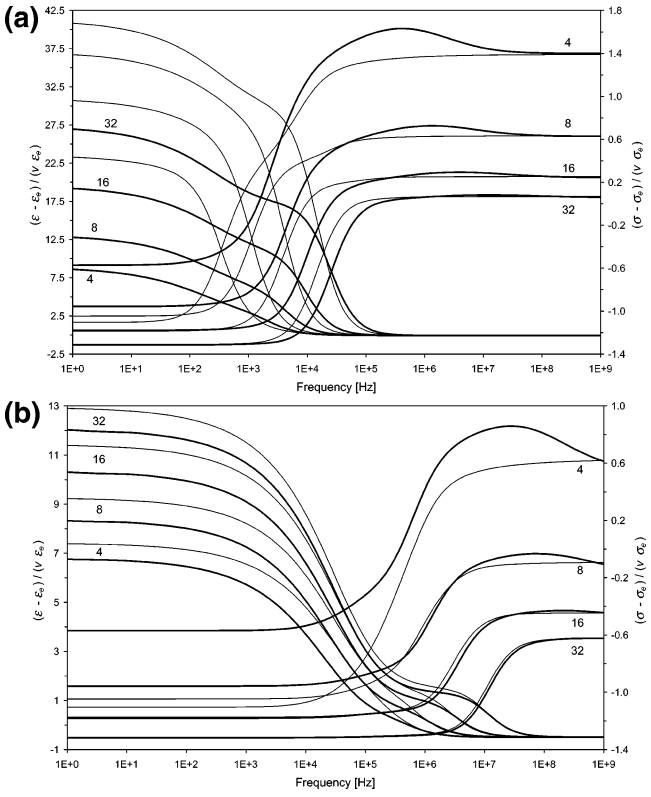

Figure 4. (a) Relative permittivity (decreasing curves) and conductivity (increasing curves) increments of suspensions of large vesicles (a = 1 μm) calculated for the indicated values of the product κa and for ζ = 50 mV. Numerical results (heavy lines) and analytical results (thin lines), eq 14, are shown. Remaining parameters are given in Table 1. (b) Same as part a but for small vesicles (a = 100 nm).

and Figure 1a. Finally, the agreement is generally poor both for the permittivity and for the conductivity in the β dispersion frequency range, because the theory strongly overestimates the membrane capacity. The situation strongly improves for a = 100 nm particles, as can be seen in Figure 3b, which shows that, in this case, the analytical expressions properly predict both the permittivity and conductivity increments, except for the highest ζ potential value.

Figure 4 shows the obtained results for different values of κa and for ζ = 50 mV. In Figure 4a, which corresponds to a = 1 μm, the numerical permittivity increment curves clearly show two dispersion regions: the LFDD and a broad dispersion made of the superposition of the β and δ processes. The analytical results show the same qualitative behavior but with a much larger amplitude of the high-frequency component. Again, this is mainly due to the overestimated value of the membrane capacity that is used in analytical expressions. The discrepancy between numerical and analytical results further worsens when the value of the product κa is decreased, as expected. As for the conductivity increment, it is fairly well represented by the analytical expressions for high values of κa but is strongly subestimated at low frequencies when κa decreases. At high frequencies, the agreement is fairly good for all values of κa.

For a = 100 nm particles, Figure 4b, the permittivity increment values become much lower than those in Figure 4a, despite having the same values of the low-frequency limit of the dipolar coefficient; see Figure 2. This phenomenon is due to the inhomogeneous nature of the particles: The β dispersion amplitude is roughly proportional to the radius of the particle,[22] so that the stored energy is lower and, consequently, the contribution of this dispersion to the low-frequency permittivity decreases for smaller particles. This greatly improves the agreement between the numerical and the analytical results at low frequencies. As for the low-frequency conductivity increment, it is much higher than the theoretically predicted value at low values of κa. This is due to the strong increase, relative to the analytical result, of the real part of the dipolar coefficient at low frequencies, Figure 2, caused by the growth of the effective particle radius.[26]

Dynamic Electrophoretic Mobility. An analytical expression for the dynamic, dimensionless electrophoretic mobility including inertial effects, can be easily obtained starting with the result deduced by O'Brien[32] for the high-frequency response

$$\mu^* \equiv \frac{3e\eta}{2kT\epsilon_e}\frac{v_v^*}{E} = \tilde{\zeta}(1 - d_H^*)\frac{\eta(1+\sqrt{i\alpha})}{\eta(1+\sqrt{i\alpha}) + \frac{i\omega}{9}a^2(2\rho_v + \rho_e)}$$

where v_v^* and ρ_v are the electrophoretic velocity and the average mass density of the vesicle and

$$\alpha = \frac{a^2\omega\rho_e}{\eta} \tag{16}$$

In this expression, deduced from the equation for the drag force acting on a spherical particle that performs low-amplitude periodic oscillations in a fluid,[33] the term $(1 - d_H^*)E$ represents the total tangential electric field on the equator of the particle.

If the low-frequency response is to be included in the calculation, two additional terms must be added.[34] The first is related to the field-induced volume charge density outside the

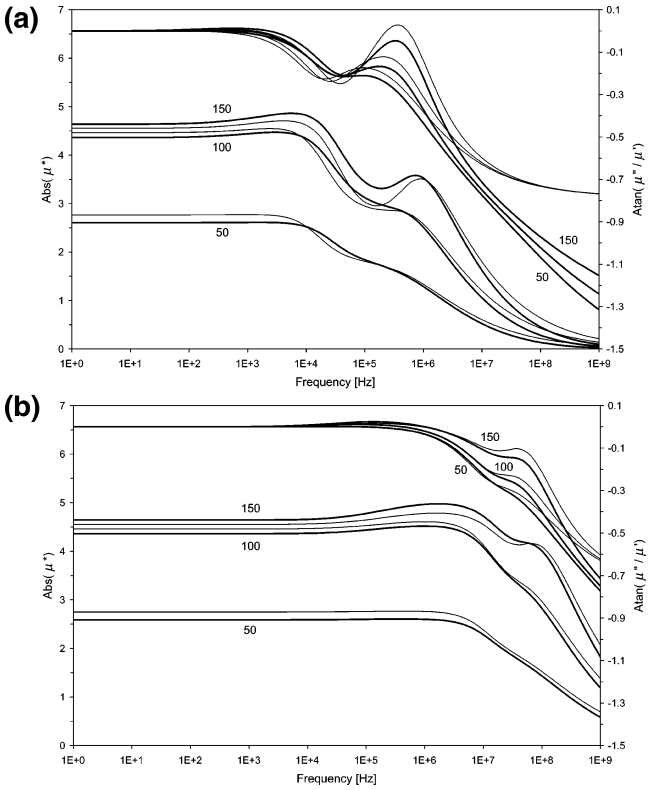

Figure 5. (a) Modulus (lower three pairs of curves) and phase (upper curves) of the dimensionless dynamic electrophoretic mobility of large vesicles ($a = 1$ μm) calculated for the indicated values of the ζ potential (in mV) and for $\kappa a = 32$. Numerical results (heavy lines) and analytical results (thin lines), eq 17, are shown. Remaining parameters are given in Table 1. (b) Same as part a but for small vesicles ($a = 100$ nm).

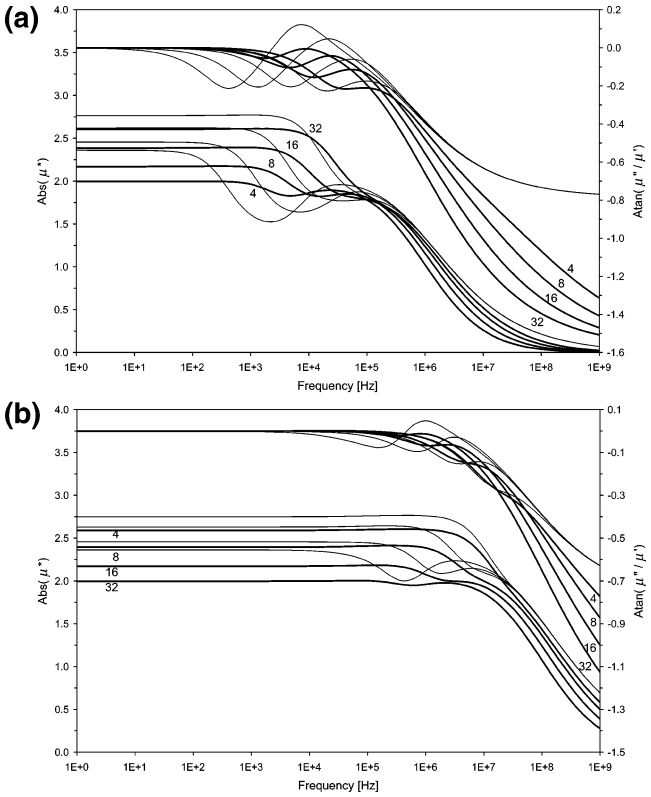

Figure 6. (a) Modulus (lower four pairs of curves) and phase (upper curves) of the dimensionless dynamic electrophoretic mobility of large vesicles ($a = 1$ μm) calculated for the indicated values of the product κa and for $\zeta = 50$ mV. Numerical results (heavy lines) and analytical results (thin lines), eq 17, are shown. Remaining parameters are given in Table 1. (b) Same as part a but for small vesicles ($a = 100$ nm).

double layer, which appears at low frequencies whenever the diffusion coefficients of counterions and co-ions differ, and contributes to the tangential electric field. The second is related to the capillary-osmotic flow along the surface of the particle, which is due to the field-induced changes of electrolyte concentration that arise at low-frequencies. This leads to

$$\mu^* = \tilde{\zeta}\left\{1 - d^* - \frac{d_{L\infty} - d_L}{H}\left[\Delta - \frac{4}{\tilde{\zeta}}\ln\left(\cosh\frac{\tilde{\zeta}}{4}\right)\right]\right\}\frac{\eta(1+\sqrt{i\alpha})}{\eta(1+\sqrt{i\alpha}) + \frac{i\omega}{9}a^2(2\rho_v + \rho_e)} \quad (17)$$

where

$$\Delta = \frac{D^- - D^+}{D^+ + D^-}$$

$$H = \frac{(R^+ - R^-)(1-\Delta^2) - U^+(1-\Delta) + U^-(1+\Delta)}{R^+(1-\Delta) + R^-(1+\Delta) + 4}$$

Figure 5 shows the obtained results for the modulus and phase of the dimensionless electrophoretic mobility calculated as a function of the ζ potential and for $\kappa a = 32$. Figure 5a, which corresponds to $a = 1$ μm particles, shows that the inhomogeneous nature of the particles leads to a marked structure of both the amplitude and the phase curves. The maxima of these curves roughly correspond to the β and δ extremes of the imaginary part of the dipolar coefficient, Figure 1a. The analytical expression reproduces these features fairly well, including the inertial drop at high frequencies, except for the high-frequency limit of the phase angle. For $\omega \to \infty$, the imaginary part of the brace in eq 17 tends to zero while the last term has the following limiting behavior

$$\frac{\eta(1+\sqrt{i\alpha})}{\eta(1+\sqrt{i\alpha}) + \frac{i\omega}{9}a^2(2\rho_v + \rho_e)} \to \frac{1-i}{\sqrt{2\alpha}}\left(\frac{2\rho_v + \rho_e}{9\rho_e}\right)$$

which shows that, according to O'Brien's theory, the limiting phase angle value is $-45°$ (0.785 rad). On the contrary, the obtained numerical results lead to values that are nearly two times larger (in modulus).

For the smaller particles, Figure 5b, the inertial drop is shifted two decades toward higher frequencies, as expected from the definition of the variable α; see eq 16. The agreement between the numerical and analytical results is quite good over the whole frequency range, except for the discrepancy in the phase angle that starts to show at the highest frequencies.

Figure 6 shows the obtained results for different values of κa and for $\zeta = 50$ mV. As can be seen, the characteristic features due to the inhomogeneous nature of the particles persist to a smaller degree while the agreement between numerical and analytical results markedly worsens. This is due to the strong influence of the β dispersion on the dipolar coefficient for small values of the ζ potential and to the limitations of the theory for small values of κa; see Figure 2.

Conclusion

In this work we present numerical results for the dielectric and electrokinetic properties of vesicles in a broad frequency

range extending from 1 Hz to 1 GHz. The calculations performed using the network method are not a simple extension of existing results, since they require new boundary conditions inside the vesicle that are associated with the convective fluid flow in the inner medium.

The obtained results show important qualitative differences with respect to suspensions of charged homogeneous particles, which are mainly due to the existence of an additional dispersion mechanism, charging of the membrane. Because of this dispersion, the spectra for particles of different size but constant ζ and κa values change their shape instead of merely shifting along the frequency axis. The additional dispersion also introduces new features in the permittivity, conductivity, and electrophoretic mobility spectra.

A comparison of the obtained numerical results with analytical predictions shows deviations that generally increase with the size of the particle and the value of the ζ potential, while they decrease with increasing κa. However, unlike the case of homogeneous particles, the agreement between numerical and analytical results is always bad in the frequency range of the β dispersion, even for moderate values of ζ and high values of κa. This is due to the existence in these systems of a second length scale: the thickness of the membrane, which is usually much smaller than the radius of the particle but comparable, nevertheless, with the Debye length.

Two additional discrepancies appear at very high frequencies, both related to inertial effects. The first is the decrease of the conductivity increment with frequency, specially pronounced for large and highly charged particles (this phenomenon is not predicted by the analytical expressions since they do not include any inertial terms). The second is a strong decrease with frequency of the phase angle of the electrophoretic mobility which, according to the obtained numerical results, could greatly exceed the theoretical limit of 45°.

These findings lead to the general conclusion that dielectric and electrokinetic measurements made on vesicle suspensions should only be interpreted using numerical, rather than analytical, results.

Acknowledgment. Financial support by the Consejo de Investigaciones de la Universidad Nacional de Tucumán, Agencia Nacional de Promoción Científica y Tecnológica, and Consejo Nacional de Investigaciones Científicas y Técnicas is gratefuly acknowledged.

References and Notes

(1) Wiersema, P. H.; Loeb, A. L.; Overbeeck, J. Th. G. *J. Colloid Interface Sci.* **1966**, *22*, 78.

(2) O'Brien, R. W.; White, L. R. *J. Chem. Soc., Faraday Trans. 2* **1978**, *74*, 1607.

(3) López-García, J. J.; Hayas, A.; Delgado, A.; Horno, J. *Recent Res. Dev. Phys. Chem.* **2000**, *4*, 309.

(4) Mangelsdorf, C. S.; White, L. R. *J. Chem. Soc., Faraday Trans.* **1990**, *86*, 2859.

(5) Wunderlich, R. W. *J. Colloid Interface Sci.* **1982**, *88*, 385.

(6) Levine, S.; Levine, M.; Sharp, K. A.; Brooks, D. E. *Biophys. J.* **1983**, *42*, 127.

(7) Sharp, K. A.; Brooks, D. E. *Biophys. J.* **1985**, *47*, 563.

(8) Ohshima, H. *J. Colloid Interface Sci.* **1994**, *163*, 474.

(9) Saville, D. A. *J. Colloid Interface Sci*. **2000**, *222*, 137.

(10) Ohshima, H. *J. Colloid Interface Sci.* **2000**, *228*, 190.

(11) López-García, J. J.; Grosse, C.; Horno, J. *J. Colloid Interface Sci.* **2003**, *265*, 327.

(12) López-García, J. J.; Grosse, C.; Horno, J. *J. Colloid Interface Sci.* **2003**, *265*, 341.

(13) López-García, J. J.; Grosse, C.; Horno, J. *J. Colloid Interface Sci.* **2005**, *286*, 400.

(14) Zimmerman, V.; Grosse, C.; Shilov, V. N. *J. Phys. Chem. B* **2003**, *107*, 14612.

(15) Zimmerman, V.; Grosse, C. *J. Phys. Chem. B* **2004**, *108*, 12617.

(16) López-García, J. J.; Horno, J.; Grosse, C. *J. Colloid Interface Sci.* **2002**, *251*, 85.

(17) Dukhin, S. S.; Shilov, V. N. *Dielectric Phenomena and the Double Layer in Disperse Systems and Polyelectrolytes*; Wiley: New York, 1974.

(18) Grosse, C.; Shilov, V. N. *J. Phys. Chem.* **1996**, *100*, 1771.

(19) Zimmerman, V.; Shilov, V. N.; López-García, J. J.; Grosse, C. *J. Phys. Chem. B* **2002**, *106*, 13384.

(20) Shilov, V. N.; Delgado, A. V.; Gonzalez-Caballero, F.; Grosse, C. *Colloids Surf., A* **2001**, *192*, 253.

(21) Grosse, C.; Arroyo, F. J.; Shilov, V. N.; Delgado, A. V. *J. Colloid Interface Sci.* **2001**, *242*, 75.

(22) Grosse, C. *Interfacial Electrokinetics and Electrophoresis*; Delgado, A. V., Ed.; Marcel Dekker: New York, 2002; Chapter 11.

(23) Simonov, V. N.; Shilov, V. N. *Kolloidn. Zh.* **1977**, *39*, 878.

(24) García, A.; Barchini, R.; Grosse, C. *J. Phys. D: Appl. Phys.* **1985**, *18*, 1891.

(25) Pedrosa, S.; Grosse, C. *J. Colloid Interface Sci.* **1999**, *219*, 37.

(26) Grosse, C.; Pedrosa, S. E.; Shilov, V. N. *J. Colloid Interface Sci.* **2003**, *265*, 197.

(27) Grosse, C.; Tirado, M.; Pieper, W.; Pottel, R. *J. Colloid Interface Sci.* **1998**, *205*, 26.

(28) Nettelblad, B.; Niklasson, G. A. *J. Colloid Interface Sci.* **1996**, *181*, 165.

(29) Hill., R.; Saville, D. A.; Russel, W. B. *Phys. Chem. Chem. Phys.* **2003**, *5*, 911.

(30) Grosse, C. *Ferroelectrics* **1988**, *86*, 171.

(31) Grosse, C.; Shilov, V. *J. Colloid Interface Sci.* **1997**, *193*, 178.

(32) O'Brien, R. W. *J. Fluid Mech.* **1988**, *190*, 71.

(33) Landau, L. D.; Lifshitz, E. M. *Mécanique des Fluides*; Mir: Moscow, 1971.

(34) López-García, J. J.; Grosse, C.; Horno, J. *J. Phys. Chem. B* **2005**, *109*, 11907.